

The muonic longitudinal shower profiles at production

S. Andringa^a, L. Cazon^a, R. Conceição^{a,*}, M. Pimenta^{a,b}

^a*LIP, Av. Elias Garcia, 14-1, 1000-149 Lisboa, Portugal*

^b*Departamento de Física, IST, Av. Rovisco Pais, 1049-001 Lisboa, Portugal*

Abstract

In this paper the longitudinal profile of muon production along the shower axis is studied. The characteristics of this distribution is investigated for different primary masses, zenith angles, primary energies, and different high energy hadronic models. It is found that the shape of this distribution displays universal features similarly to what is known for the electromagnetic profile. The relation between the muon production distribution and the longitudinal electromagnetic evolution is also discussed.

Keywords: Extensive Air Shower, Longitudinal Profile, Muon Production Depth, Electromagnetic component

1. Introduction

The origin and mass composition of the most energetic particles in the Universe, the Ultra High Energy Cosmic Rays (UHECRs), remains a mystery. These particles reach the Earth with a very scarce flux. Fortunately, their interaction with the atmosphere molecules produces huge cascades of particles, known in the literature as Extensive Air Showers (EAS), allowing their detection. The detection of these showers is usually done by measuring the charged particles that arrive at the ground, or, in moonless nights, the development of the shower can be followed through the fluorescence light produced by the EAS.

While the arrival direction of the UHECRs can be easily obtained using any of the techniques mentioned, the mass composition of the primary particle is much more difficult. The shower observables connected to the type of primary particle are also sensitive to the physical interactions that occur during shower development. The hadronic interactions at high energies are described through phenomenological models that are fitted to the available accelerator data and extrapolated several orders of magnitude to the UHECRs energies. Moreover, the accelerators have difficulty to reach the most important region for the characterization of the EAS development, the forward region, causing the uncertainties on the extrapolation to be higher.

Contrary to the fluorescence light, which is dominantly produced by low energy electrons in secondary electromagnetic cascades, ground signals are sensitive to muons arriving at ground directly from their production point at different depths, thus imaging the hadronic cascade. Although

*Corresponding author

Email address: ruben@lip.pt (R. Conceição)

many of the muons will decay before reaching the ground, that effect can be accounted for in analysis by using a proper transportation model [1]. In the following, we will consider all the produced muons, characteristic of the shower properties and independent of the detection conditions.

The analysis of muons at ground has been used previously to study high energy hadronic models and primary composition of cosmic rays. The number of muons at a given distance from the core is used in [2], showing that at very high energy the data can not be explained by the available models; in [3] the timing signals have been translated to a production depth to analyze the energy evolution of the depth of maximum as in the electromagnetic profile, showing that the trends observed are compatible in both cases, and giving access to higher statistics at high energies - although the analysis is restricted to a narrow observation angle window. The simultaneous analysis of the electromagnetic calorimetric energy and ground signals has been used in [4] to correct for the “invisible” energy carried by muons (and neutrinos), showing that the energy determination can be improved on an event-by-event basis.

To our knowledge, there is no systematic study of the distribution of the muon production, independent of detector effects, and we will proceed to identify its main characteristics. This is directly related to the hadronic shower profile, inaccessible experimentally. Thus, in this article, our main objective is to characterize not only the more general features of the muon longitudinal profile at production, namely the depth of the profile maximum, X_{max}^μ , and its corresponding value, N_{max}^μ , but also its shape. The comparison with the features observed in the energy deposit profile, referred to in this paper as electromagnetic profile, will be made whenever relevant.

Since in this study we are only interested on the longitudinal profile, and not the transverse distributions, we used the hybrid shower simulation CONEX [5, 6] (version v2r3). This program combines Monte Carlo simulation with one-dimensional cascade equations making it very fast and allowing the production of large samples of showers. CONEX gives as output the energy deposit profile as a function of depth (X), the number of muons produced as a function of X , and the more extensively used number of muons along the shower axis. Note that this last one, the instant number of muons as a function of the shower depth, is in first approximation the cumulative of the number of muons produced, apart from the muons that decay. We will concentrate our study in the muon production profile. In this work we study the dependence of the muon shower production profile on the primary mass composition (proton and iron), zenith angle, different hadronic models, in particular QGSJet-II.03 [7, 8] and EPOS1.99 [9] and on the primary energy. For each case samples of 50000 showers were generated. The ground was set at 4000 g cm^{-2} to avoid an abrupt termination allowing us to see the full tail of the shower profile as if it had a very inclined zenith angle, θ .

The paper is organized as follows: in Sec. 2 the main features of the muon production shower profile are studied and related to the electromagnetic profile; the shape of the profile is characterized in Sec. 3 and here is shown that, similarly to what happens in the electromagnetic case, this profile exhibits an universal behavior when put in the coordinates, $X' \equiv X - X_{max}$ and $N' \equiv N/N_{max}$; in section 4 the impact of the muon energy threshold on the longitudinal profile is investigated; the extraction of more information on basic variables like the total number of muons or the point of first interaction are discussed in Sec. 5; the paper ends the with conclusions and prospects.

2. Longitudinal shower profiles

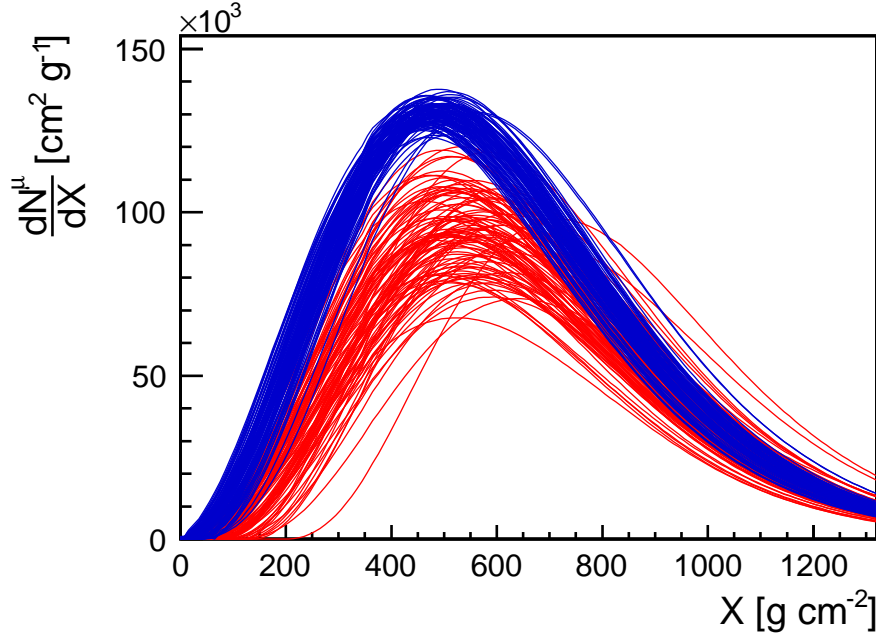
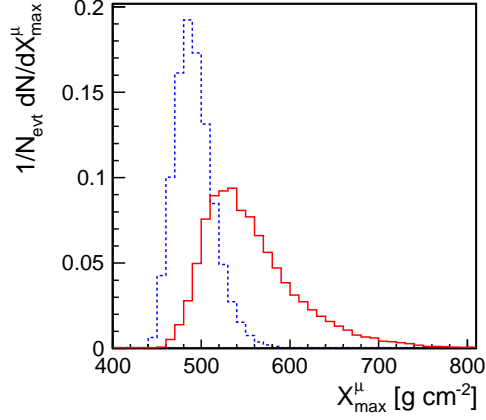


Figure 1: Muon production shower profiles as a function of depth (X), for proton (red) and iron (blue) primaries at $E = 10^{19}$ eV.

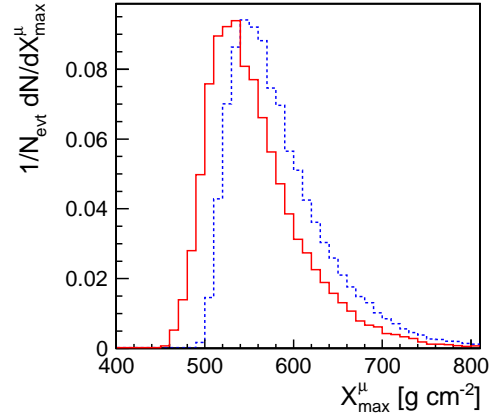
The muon production longitudinal profile for proton induced showers (in red) and iron primaries (blue) at $E = 10^{19}$ eV is shown in figure 1. These profiles were obtained with CONEX where the minimum energy threshold for muons is 1 GeV (the effect of this cut is discussed in Sec. 4).

The shower profiles reflect the properties of the first stages of the hadronic interaction, in particular the first one, which can not be observed directly. They are thus very different for proton and iron initiated showers, as shown in Fig. 1. Compared to proton showers, iron showers have a higher number of muons, which is readily seen just by looking at the maximum of the profile, N_{max}^{μ} . In iron showers more charged pions are produced: low energy pions will give rise to muons as they decay, others will interact producing even more pions that will decay later, but in a very fast process. Protons exhibit much more fluctuations: the energy degradation is slower, thus less muons are produced and more spread along the shower axis.

Neutral pions of all energies decay immediately and around 90% of the primary energy will feed electromagnetic cascades; the energy deposit in the atmosphere is dominated by low energy electrons after a few radiation lengths. All of the sub-cascades add up to give a well defined maximum height of the profile. Not only the integral of the profile is a good calorimetric measurement of the energy of the primary particle (which must be corrected for the muons and accompanying neutrinos which reach the ground), but also the maximum of the profile is quite stable, within 5% [10] for both primaries. Because it corresponds to a much higher number of particles than those in

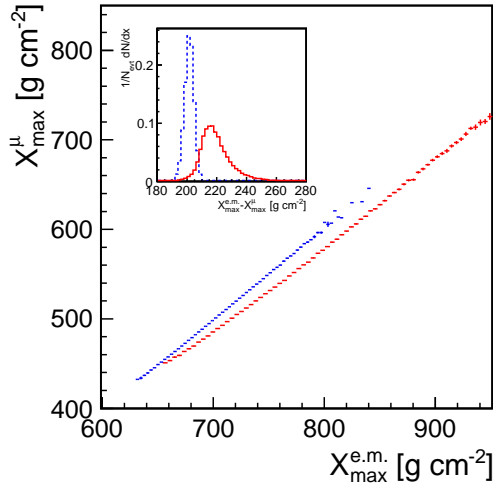


(a)

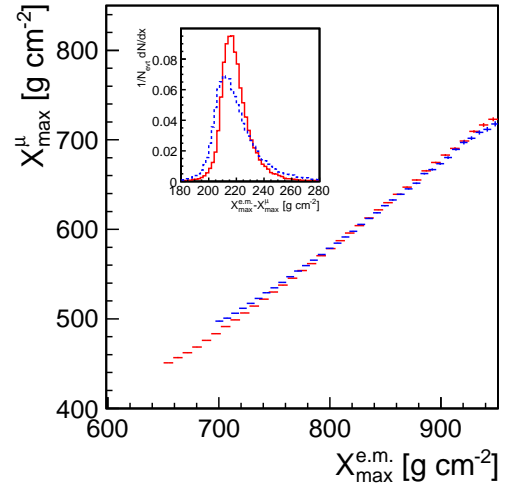


(b)

Figure 2: X_{max}^{μ} distributions of muon production longitudinal profiles for: (a) different primaries - the proton distribution is in red while iron is in blue; (b) high energy hadronic models - QGSJet-II is in red and EPOS1.99 is shown as blue.



(a) Proton is the red (full) line and iron the blue (dashed) line.



(b) QGSJet-II is the red (full) line and EPOS1.99 the blue (dashed) line.

Figure 3: Relation between Muon production X_{max}^{μ} and electromagnetic $X_{max}^{e.m.}$, for $E = 10^{19}$ eV showers. The difference between the two X_{max} are shown in the inset plots. In (a) the dependence on primary mass is shown, while in (b) the dependence on high energy hadronic models (for proton induced showers).

the muon production profile this number has much less fluctuations. In the electromagnetic case, it is the depth of the maximum, $X_{max}^{e.m.}$, that gives more information about the other shower properties.

The depth of the maximum of a shower, X_{max} , is determined by the depth of first interaction, X_1 , but also the subsequent development, ΔX . The variation of the first is common to both the electromagnetic and muon profiles, while the later is different. Iron primaries have a larger cross-section and higher multiplicity and both effects contribute to make the maximum depth average, $\langle X_{max} \rangle$, lower and $RMS(X_{max})$ smaller than the corresponding proton values. In Fig. 2, we show the X_{max}^μ distributions for the muon production profiles, comparing different primaries and different hadronic models. The features are similar to the ones of the electromagnetic $X_{max}^{e.m.}$, and the correlations between muonic and electromagnetic maxima can be seen in Fig. 3, together with the differences. Notice that the difference is only sensitive to ΔX , thus it is giving information about the history of pion production.

The electromagnetic maximum is reached around 200 g cm^{-2} later, after the energy is degraded to a large number of electrons (which will then stop multiplying), while the muonic profile has a maximum when the hadronic shower is still important (and will start decreasing as pions stop being produced). The correlation between the two X_{max} is similar between hadronic models, which means that the different treatments of pions are reflected in both profiles. The difference between primaries is much larger than between hadronic models as it depends critically on the multiplicity of pion production and the corresponding energy spectrum in the first interactions. The difference between electromagnetic and muonic X_{max} , shown as an inset plot of fig. 3, also changes between primaries – by around 30 g cm^{-2} in the average separation – which means that although related, the electromagnetic and muonic profiles give some independent information.

3. Universality of the longitudinal profile shape

In Fig. 4, the profiles are expressed in $X' \equiv X - X_{max}$ and $N' \equiv N - N_{max}$. The obtained shape is rather universal, similarly to what happens to the energy deposit profile. It can be useful to use the average shape in order to determine the two main parameters from a fit with a reduced set of data. On the other hand, there can be extra information on the shape, and we can now construct average profiles to look in detail for differences between primaries and hadronic models. From that comparison, in fig. 5 (left), it is clear that iron showers develop faster, with almost no difference between models.

The dependence on zenith angle is also studied. Muon production depends on the competition between the pion interaction and decay lengths. The bigger the energy the most probable is for a pion to interact instead of decaying into a muon, but that dependence can not be expressed in X alone, as the decay length is independent of the atmospheric density. Nevertheless, the average muon profile, in figure 5 (right), is still rather universal. There are, as expected, some minor violations to this universality that are more important in the early phase of the shower.

This quasi-universal shape is compared to the electromagnetic shape in fig. 6. The differences are clear: the muonic profile has a steeper growth and is more asymmetric. Both profiles are fitted with a function inspired by the Gaisser-Hillas parametrization, but re-written in terms of a Gaussian width L and a distortion parameter R , from [10],

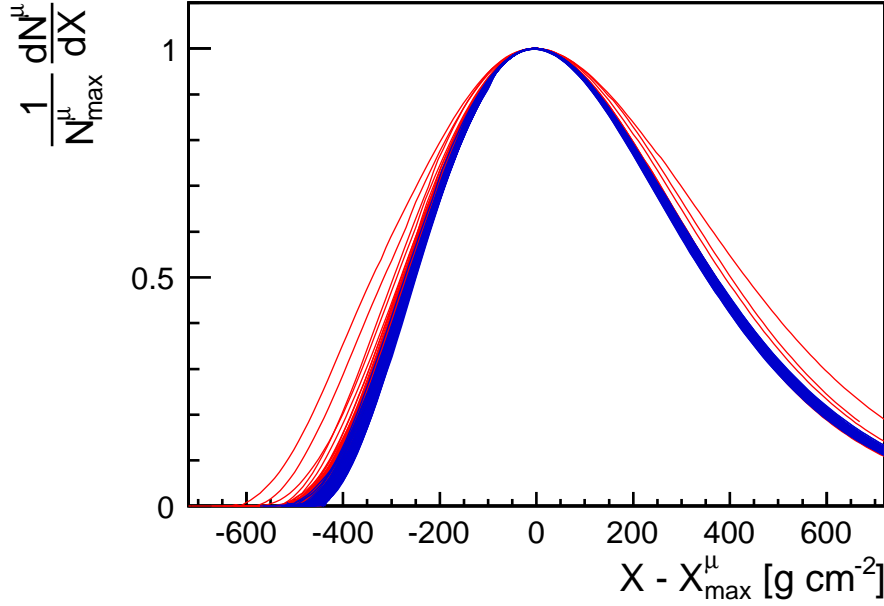


Figure 4: Muon production shower profiles from proton (red) and iron (blue) primaries, in (X', N') coordinates. The same showers used to build Fig. 1 are used here.

$$N' = \left(1 + \frac{RX'}{L}\right)^{R-2} \exp\left(-\frac{X'}{LR}\right). \quad (1)$$

We conclude that the muon production profile can be well described with the same function as used for the electromagnetic profile, as seen in figure 6. It should be noted that the region around the maximum is better described by a Gaisser-Hillas function for the electromagnetic profile. However, the full profile description is better achieved through the Gaisser-Hillas parametrization for the muon production profile. This is because the end tail of the energy deposit profile has important indirect contributions from muon decays. For showers initiated by protons of 10^{19} eV, the width of the average muon production profile is larger by 40 g cm^{-2} and the distortion is almost doubled with respect to the electromagnetic profile. The average values and dispersion of these parameters evolve slowly with $\log(E)$, as shown in fig. 7 for the case of proton showers.

The differences found for proton and iron profile shapes can now be quantified in these parameters, with the corresponding distributions shown in fig. 8. The asymmetry is almost the same for both primaries, the difference in means being well below the 5% dispersion in each sample. Since R only affects the tails it can easily be fixed in the following analysis. The Gaussian width, on the other hand, has different means for each primary, well above the single primary dispersion, and consistently for the two hadronic models studied. So, it is a new variable for mass composition studies, and fairly model independent.

Clearly L^μ is giving information about ΔX^μ , as it has been obtained starting from $X - X_{max}^\mu$,

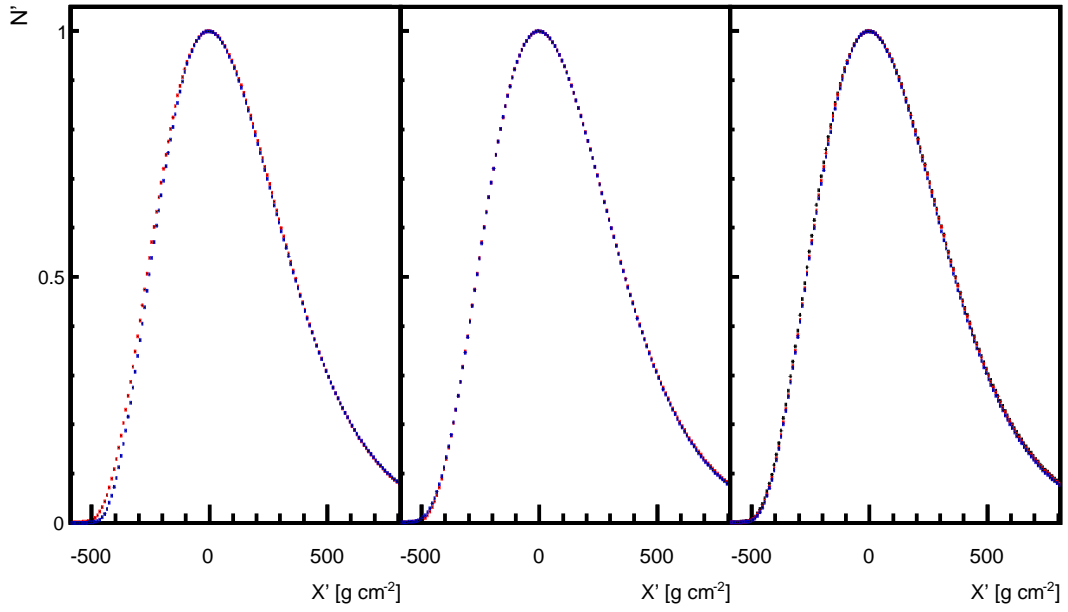


Figure 5: Average muon production longitudinal profile in (X', N') coordinates: (left) dependence on primary mass - proton (red) and iron (blue); (middle) dependence on the hadronic model - QGSJet-II (red) and EPOS1.99 (blue); (right) dependence on the zenith angle, θ - Black for $0^\circ < \theta < 10^\circ$, red for $30^\circ < \theta < 40^\circ$, and blue for $45^\circ < \theta < 55^\circ$.

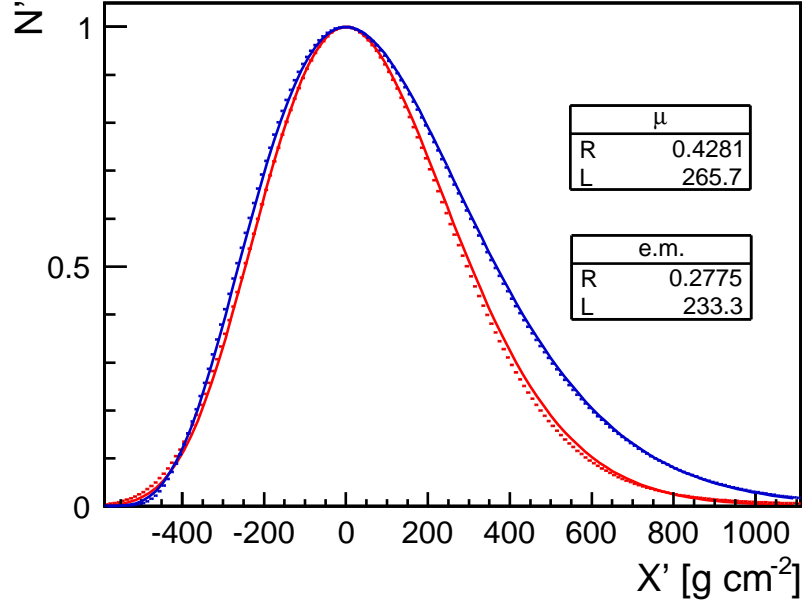


Figure 6: Average shower profiles for proton primaries at $E = 10^{19}$ eV, with QGSJet-II, in (X', N') coordinates. Comparison between electromagnetic (in blue) and muonic (in red) shape features. The lines correspond to fits using a Gaisser-Hillas function (2 parameters). The fit results are given in the plot for the electromagnetic (e.m.) and muonic (μ) profiles.

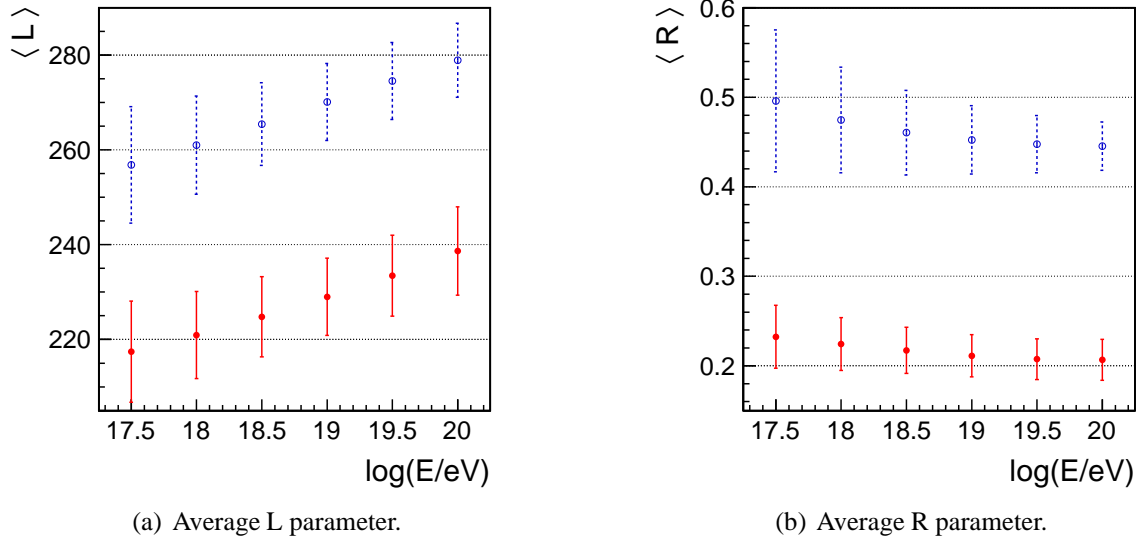


Figure 7: Shape parameters dependence on the shower energy. The shape parameters for the electromagnetic profile are shown in red (full) line while the muon production is shown in blue (dashed). The error bars represent the RMS of the corresponding distribution. The showers were generated using QGSJet-II as high energy hadronic model.

with no memory of X_1 . It can be measured with ground detectors only. L^μ can be combined with X_{max}^μ to obtain X_1 similarly to what is made for the electromagnetic case [10].

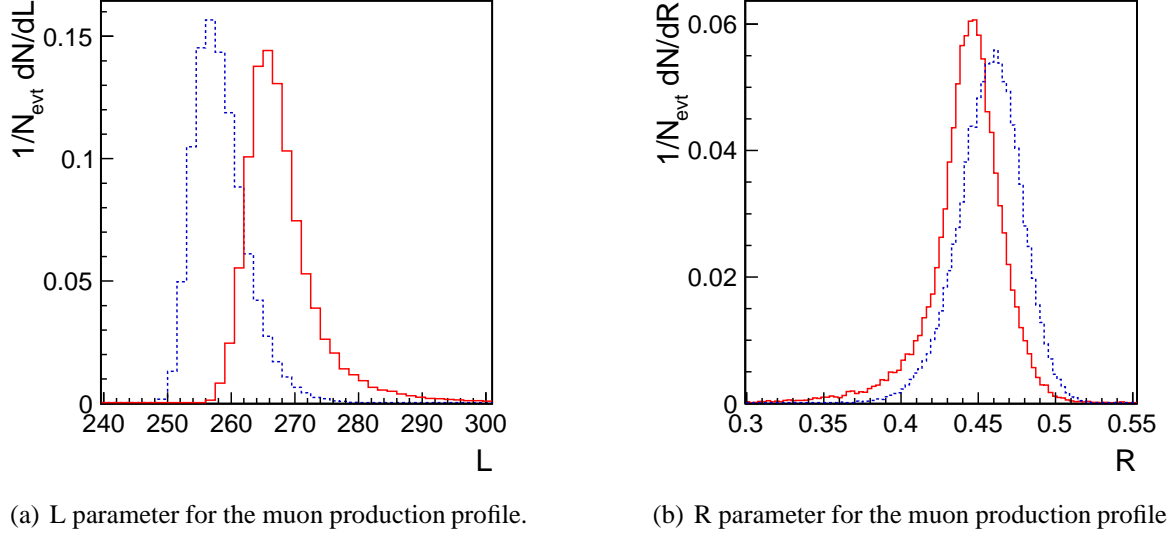


Figure 8: Shape parameters for different primaries: proton (red/full) and iron (blue/dashed), at $E = 10^{19}$ eV, and with QGSJet-II.

The relation between the shapes of the electromagnetic and the muon production profile of each individual event can be seen in fig. 9. Here, $(L^{e.m.}, R^\mu)$ are fixed to its corresponding average values, and most of the information is kept in a single, most sensitive variable. The correlation is rather strong in the most populated region of $(R^{e.m.}, L^\mu)$. Moreover, it is almost independent of the primary mass composition, making it very useful for hybrid analysis, where both profiles are reconstructed, and one can be used to constrain the other.

4. Dependence on the energy cutoff

The previous studies were done with CONEX generated profiles, including a muon energy threshold of 1 GeV¹. The final threshold for observation depends not only on the detector used, but also on the zenith angle of the shower, and within the same shower will be different for different depths. It is worth verifying how do the previous conclusions depend on the threshold used.

Fig. 10 is done for proton showers generated with CORSIKA [11] (version 6.980), which allows the setting of lower energy thresholds (but is much slower, so there is less statistics). This version was modified in order to obtain the muons at production. We first checked that the results obtained with CORSIKA and CONEX are compatible at 1 GeV. From Fig. 10(a) is clear that N_{max}^μ changes drastically with the cut considered, and also X_{max}^μ has some variation, since low energy

¹minimum value permitted in CONEX simulations.

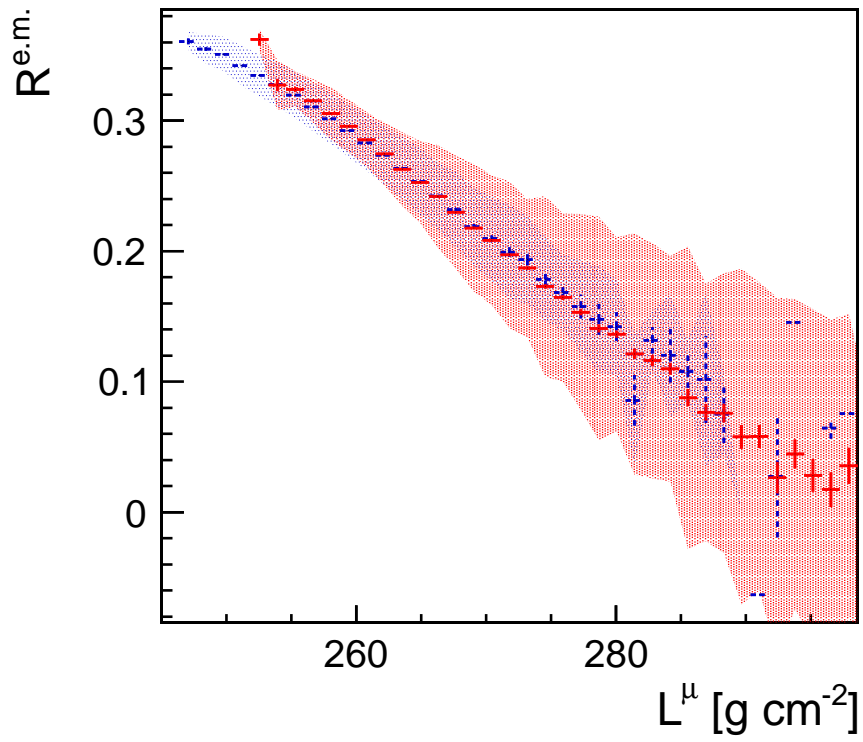


Figure 9: Correlation between the electromagnetic profile shape (characterized by $R^{e.m.}$) and the muon production profile shape (represented by L^μ). The results are shown for proton (red/full) and iron (blue/dashed) induced showers, at $E = 10^{19}$ eV, and with QGSJet-II.

muons can be produced until much later. However all the profiles are still described by a Universal Shower Profile, which can still be described by L and R . From Figure 10(b) we can infer that L gets smaller as the energy increases, and the R gets slightly larger.

To extract the full information about the muon production profile, there will be need for a propagation model taking into account the muon energy from production to detection [1]. It will also be useful to have a detector which can select muons with a minimum energy threshold. The systematic uncertainties coming from the translation between the modeled distribution and the detected one will thus be minimized. These systematic uncertainties can be estimated directly with the data by comparing different detection conditions, selected by zenith angle bins or by individual detectors seeing the same event. In any case, the ideas of universality and the new composition variables are still valid, even if the method has to be calibrated for different detection conditions using data.

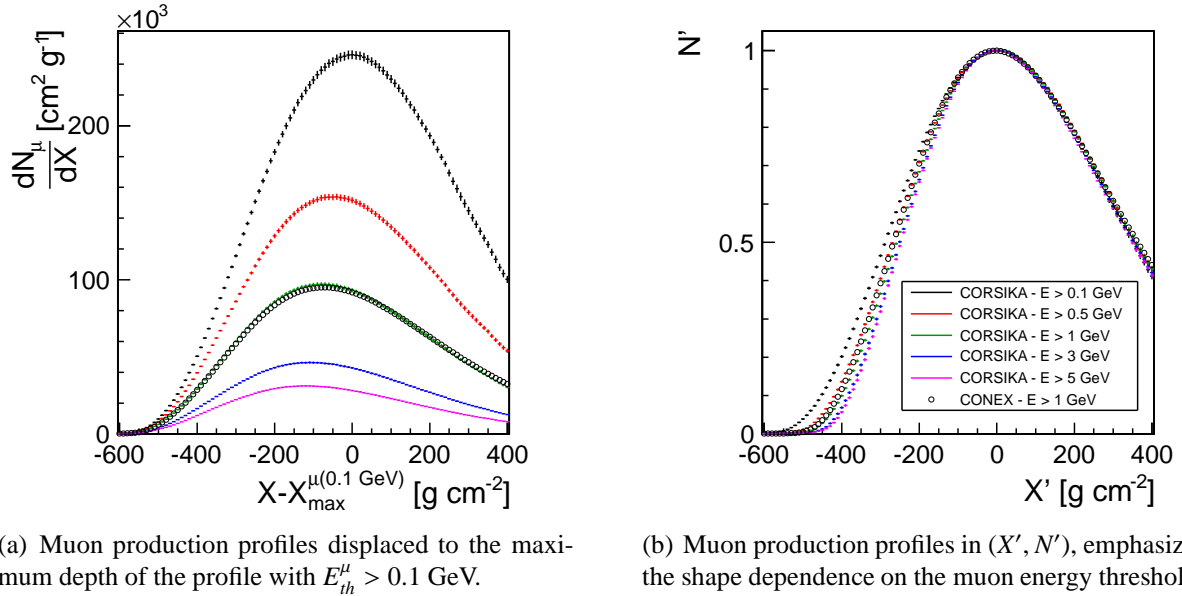


Figure 10: Average muon production profile as a function of the muon energy threshold, for proton induced showers at $E = 10^{19}$ eV, with QGSJet-II. The CORSIKA showers are the average of 100 events while CONEX has 50000 events.

5. Total Number of Muons and Muons from the First Interaction Point

The integral of a Gaisser-Hillas profile is readily obtained from $\int N^{\mu} dX = \sqrt{2\pi} \cdot N_{max} \cdot L \cdot f(R)$, in which $f(R)$ is a small correction of around 1.02 for $R \sim 0.5$. This gives the energy in electromagnetic profiles, and the total number of produced muons (above a given energy threshold) for the muon production profiles. So, by using the above formalism, the total number of muons can be obtained with a small uncertainty, just by detecting the region of shower maximum, in an event-by-event way. Moreover, as seen before, at first order, L^{μ} is constant, and consequently N_{max}^{μ}

can be used itself as a measurement of the total number of muons produced during the shower development.

This is reasonably different from the usual muon counting methods, which deal with the muons observed at ground, more dependent on detection conditions and harder to relate to the underlying physics. Of course, for this the muon transport model has to take into account the produced muon spectrum, keep track of the muon decays through the atmosphere and detection efficiencies have to be considered.

On the other hand, when working in X' , the shape variables L and R become a measurement of ΔX ; together with X_{max} they can be used to calculate the point of first interaction, $X_1 = X_{max} - \Delta X$. For the muon production profile, R can be fixed, and L can be measured close to the shower maximum, so that at least a part of the variation on ΔX can be accounted for for most of the measured events.

In fact, the profile of muons starts much earlier than the energy deposit profile, with muons being observed directly from the first few interactions and with a much steeper rise (as illustrated in Fig. 11), so it should be easier to extrapolate the profile back and reconstruct X_1 almost directly. The fraction of produced muons that will decay before reaching the ground level increases with the zenith angle θ . Hence, the energy threshold for the muon to reach the ground depends also on this quantity, θ . Studies of the distribution of the first muons as a function of θ can thus give some insight about the parent pion energy distributions in the high energy interactions.

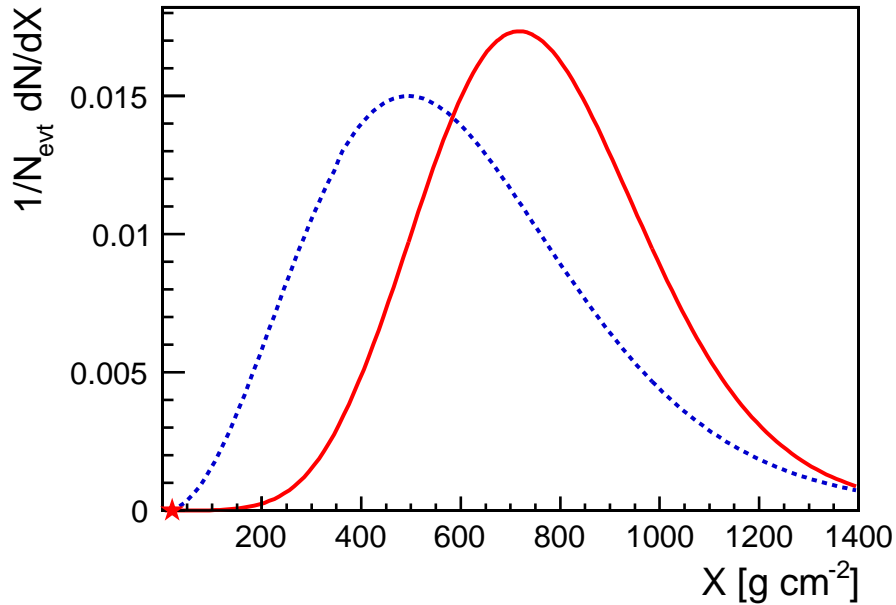


Figure 11: Electromagnetic (blue) and muon production (black) longitudinal profiles of a single *typical* EAS at $E = 10^{19}$ eV. The shower was produced using QGSJet-II as high energy hadronic model. Both profiles were normalized to the area. The first interaction point is shown as a red star.

6. Conclusions and Prospects

The muon production longitudinal profile of air showers is a true characteristic of the shower (independent of detection conditions), described by the same parametrization as the electromagnetic profile. It gives new primary mass composition variables which are fairly independent of the high energy hadronic interaction model: the X_{max}^μ and the shape variable L^μ . These variables can be combined to obtain the point of first interaction. The normalization of the profile gives also access to the total number of produced muons, which is known to be an important variable, both for primary composition and high energy hadronic model studies. For its reconstruction a muon transport model will be needed but the associated systematics uncertainties can be estimated in data.

Joining all the information with the electromagnetic profile will give rise to extra variables, mostly sensitive to the shower development characteristics, and to a more precise understanding in terms of energy distribution along the shower development. With the higher number of available observables, using profiles which are independent of the detection conditions and more directly related to the hadronic cascade, cosmic rays become increasingly useful for the study of particle physics at the highest energies.

Acknowledgments

We would like to thank J. Alvarez-Muñiz, R. Engel and the Auger LIP group for careful reading the manuscript. This work is partially funded by Fundação para a Ciência e Tecnologia (CERN/FP11633/2010 and SFRH/BPD/73270/2010), and fundings of MCTES through POPH-QREN-Tipologia 4.2, Portugal, and European Social Fund.

References

- [1] L. Cazon, R. Conceição, M. Pimenta, E. Santos, Transport of muons in Extensive Air Showers - Submitted to Astropart. Phys.
- [2] J. Allen, for the Pierre Auger Collaboration, Interpretation of the signals produced by showers from cosmic rays of 10^{19} -eV observed in the surface detectors of the Pierre Auger Observatory; arXiv:1107.4804.
- [3] D. Garcia Gamez, for the Pierre Auger Collaboration, Measurement of atmospheric production depths of muons with the Pierre Auger Observatory; arXiv:1107.4804.
- [4] A. G. Mariazzi, for the Pierre Auger Collaboration, A new method for determining the primary energy from the calorimetric energy of showers observed in hybrid mode on a shower-by-shower basis; arXiv:1107.4804.
- [5] T. Pierog, et al., First results of fast one-dimensional hybrid simulation of EAS using CONEX, Nucl. Phys. Proc. Suppl. 151 (2006) 159–162. ; arXiv:astro-ph/0411260.
- [6] T. Bergmann, et al., One-dimensional hybrid approach to extensive air shower simulation, Astropart. Phys. 26 (2007) 420–432. ; arXiv:astro-ph/0606564.
- [7] S. Ostapchenko, Non-linear screening effects in high energy hadronic interactions, Phys.Rev. D74 (2006) 014026. ; arXiv:hep-ph/0505259, doi:10.1103/PhysRevD.74.014026.
- [8] S. Ostapchenko, On the re-summation of enhanced Pomeron diagrams, Phys.Lett. B636 (2006) 40–45. ; arXiv:hep-ph/0602139, doi:10.1016/j.physletb.2006.03.026.
- [9] K. Werner, F.-M. Liu, T. Pierog, Parton ladder splitting and the rapidity dependence of transverse momentum spectra in deuteron-gold collisions at RHIC, Phys.Rev. C74 (2006) 044902. ; arXiv:hep-ph/0506232, doi:10.1103/PhysRevC.74.044902.

- [10] S. Andringa, R. Conceição, M. Pimenta, Mass composition and cross-section from the shape of cosmic ray shower longitudinal profiles, *Astropart.Phys.* 34 (2011) 360–367. doi:10.1016/j.astropartphys.2010.10.002.
- [11] D. Heck, et al., CORSIKA: A Monte Carlo code to simulate extensive air showers, FZKA Report 6019.